IEEE Access
Multidisciplinary | Rapid Review | Open Access Journal

Received 27 July 2022, accepted 12 August 2022, date of publication 17 August 2022, date of current version 23 August 2022.

Digital Object Identifier 10.1109/ACCESS.2022.3199361

RESEARCH ARTICLE

A 60 GHz Rhombic Patch Array Antenna With High Gain, Low Sidelobe Level, and Reduced Array Area

CHI-EN TSAI[1], HUAYAN JIN[2], (Member, IEEE), CHAO-HSIANG LIAO[3], CHUNG-YI LI[1], (Senior Member, IEEE), WEI-CHIH CHANG[1], HUAI-EN LIU[1], AND KUO-SHENG CHIN[1], (Senior Member, IEEE)

[1]Department of Electronic Engineering, Chang Gung University, Taoyuan 333, Taiwan
[2]Key Laboratory of RF Circuits and System of Ministry of Education, Hangzhou Dianzi University, Hangzhou 310018, China
[3]Wireless Laboratory, SGS Taiwan Ltd., New Taipei 24803, Taiwan

Corresponding author: Kuo-Sheng Chin (kschin@mail.cgu.edu.tw)

This work was supported in part by the Ministry of Science and Technology under Grant MOST 110-2221-E-182-022; and in part by Chang Gung University, Taiwan, under Grant BMRP 903.

ABSTRACT This work designs a 60 GHz rhombic patch array antenna with high gain, low sidelobe level (SLL), and reduced array area. This antenna consists of eight linear serial arrays with varying number of patches. A slot-coupled center-fed structure of substrate-integrated waveguide (SIW) is designed to simplify the complex feed network required for direct excitation of planar arrays and reduce insertion loss. The rhombic configuration utilizes the quantity ratio of patches for equivalent taper excitation to reduce SLL, rather than the use of tapered width as in traditional designs, which can achieve high gain and avoid cumbersome resizing of patches and connecting lines. An array factor analysis method is proposed to predict the SLL of the antenna. To form a planar array and further reduce the H-plane SLL, a −25-dB Dolph-Chebyshev SIW feed network is constructed. The measured gain of the rhombic array antenna is 18.2 dBi, and the E-plane and H-plane SLLs are less than −20 dB and −25 dB, respectively. This work also simulates a reference uniformly excited high-gain 8 × 10 array antenna. Compared to this reference antenna, the proposed rhombic array antenna has similar simulated gain but much lower SLL and 23% smaller array area.

INDEX TERMS High-gain antenna, low sidelobe, millimeter-wave antenna, rhombic array antenna, 60 GHz antenna.

I. INTRODUCTION

Communication standards such as IEEE 802.11ad/WiGig and 802.11ay use carrier spectrum around 60 GHz because the 60-GHz band enables high throughput wireless communication applications. For wireless communication, the main lobe of the antenna is conducive to receiving/transmitting signals, while the sidelobes may reduce the antenna gain and increase communication interference. Therefore, reducing the sidelobe level (SLL) is one of the main issues for 60-GHz array antenna designs.

The associate editor coordinating the review of this manuscript and approving it for publication was Debabrata Karmokar.

In recent years, many low-SLL antennas have been developed [1], [2], [3], [4], [5], [6], [7], [8], [9], [10], [11], [12], [13], [14], [15], [16], [17]. To reduce SLL, the current amplitude of each element antenna needs to be excited with taper distribution. There are two main synthetic methods to achieve low SLLs. One way is to use deterministic designs, such as using Taylor, Chebyshev, and other mathematical function distributions, while the other is more stochastic, such as using genetic algorithms and differential evolution algorithms (DEA). Two commonly used antenna structures are width-tapered patches and position-offset slots. The 28 GHz patch array in [1] adopted Taylor distribution, which can achieve gain and SLL of 13.97 dBi and

−20 dB, respectively, but the required cross-layer feed network design is complicated. In [2], the antenna was designed with radiation slots on substrate-integrated waveguide (SIW) lines, which used the Elliott's design procedure to achieve the Taylor distribution. The measured SLL was −32.3 dB. The patch array in [3] was non-uniformly positioned, and the particle swarm optimization was used to find the optimal patch positions, which reduced the SLL by 7.57 dB. In [4], a circularly-polarized leaky-wave antenna was designed based on substrate-integrated image guide, and an SLL of −19.1 dB was achieved. A phased array antenna in [5] achieved low SLL through a random sequential rotation technology. The 38.5 GHz antenna in [6] was arranged in a honeycomb array to suppress SLL. In [7], a 28 GHz dual-polarized slot array antenna was carried out through gap waveguide technology with multi-layer feed network. The SLL was reduced up to −19.5 dB. Microstrip magnetic dipoles were used to design phased array antennas in [8], where attenuators were used to achieve amplitude taper distribution. The SLL at ±77° could be lower than −9 dB, and was less than −15 dB at other angles. Both the array antennas in [9] and [10] adopted cavity-backed slot structures, and the amplitude distribution was controlled through the matching vias in the cavity [9] or through the slot size [10], thereby reducing SLL. A 60 GHz series-fed waveguide reflection-canceling slot array antenna [11] was designed to achieve Taylor excitation by suppressing the slot reflection. Some studies propose to adjust the width of patches and feed lines to achieve the desired current distribution. In [12], a 1 × 8 traveling wave array antenna adopted serial microstrip lines and inset-fed tapered patches, which can suppress the reflection of antenna elements and control the radiated power. In [13], a W-band 16 × 26 array antenna achieved low SLL through serial patches with tapered widths. In [14], an 8-element coupled patch array antenna with non-uniform spacing and groove length was reported. The design method is complicated. In [15], a CP low-SLL antenna array for electronic toll collection applications was designed based on the weighted constrained method of the maximum power transmission efficiency. The measured results indicated a SLL below −30 dB. Some studies have proposed rhombic configurations to improve the antenna performance [16], [17], [18], [19], [20]. The antenna in [16] compared the microstrip reflector arrays with different aperture shapes. The area of the rhombic aperture is the smallest, and the SLL can be reduced by 3.7 dB compared with the square aperture. In [17], a rhombic patch array was proposed to reduce SLL by arranging the number of patches close to a binomial distribution. But only an approximate analysis method was developed. The planar metamaterial antenna in [18] designed an offset-fed rhombic split ring to increase the bandwidth, but not for SLL reduction. In [19], a rhombic grid array antenna was proposed to increase the antenna gain. Although [20] qualitatively described the calculation principle of the array factor of planar arrays with different shapes, it did not give a specific analytical formula that can be applied to the proposed rhombic array antenna. Most of the aforementioned low-SLL antenna structures are quite complex, with low gain and operating frequencies below 60 GHz. Therefore, the practical realization of low-SLL antenna arrays is still very challenging.

Take the tapered excitation method as an example, which requires each antenna element to have different weight coefficients. Conventionally, series-fed patch arrays with tapered widths are often used to achieve the tapered excitation [12], [13]. Because low sidelobe patterns are very sensitive to the phase variations of the radiating elements, these designs require cumbersome resizing of patches and connecting lines to achieve the desired weight coefficients and same phase. If the operating frequency is high and the array is large, the design of the feed network will be very difficult. Another problem with most reported low-SLL antenna designs is that the gain drops significantly.

To solve these problems, this work presents a 60-GHz high-gain low-sidelobe rhombic array antenna. The following innovative techniques have been used in this design, which are helpful to improve the performance of conventional patch array antennas:

(1) Rhombic array configuration: This work introduces a rhombic array configuration, which utilizes the quantity ratio of serial patches to design a 60-GHz planar array antenna with easy design, high gain, and low SLL. The proposed rhombic array utilizes the equivalent taper excitation caused by the quantity ratio of patches to reduce SLL, rather than the use of tapered width as in traditional designs, which can achieve high gain and avoid cumbersome resizing of patches and connecting lines;

(2) Analytical formula for rhombic array antenna: To the best of the authors' knowledge, there is no analytical formula for the proposed rhombic array antenna to calculate its radiation pattern. In this work, an array factor based analytical formula is developed to calculate the radiation pattern and SLL of the rhombic array antenna. The detailed analytical formula and analysis results are given, which can accurately predict the design results. This formula is proposed for the first time and is quite novel;

(3) Feed network design: The rhombic array is assembled using linear serial patch arrays with four different numbers of elements. A SIW anti-phase slot-fed structure is designed to feed signal in the center of the linear serial patch array. The current direction of each patch is consistent, so as to achieve in-phase radiation. A −25-dB Dolph-Chebyshev SIW eight-way feed network is designed in the H-plane direction, which can further suppress the sidelobe of the array;

(4) Low sidelobe, high gain, and reduced array area: A complete rhombic array antenna with RWG-to-SIW transition was fabricated for demonstration. The measured results show that the proposed design can achieve a gain of 18.2 dBi and low SLLs of −20 dB

and −25 dB in the E-plane and H-plane directions, respectively. For comparison, this work also simulates a uniformly excited 8 × 10 rectangular array antenna. Compared to this reference antenna, the proposed rhombic array antenna has similar simulated gain but much lower SLL and 23% smaller array area.

The rest of this paper is organized as follows: The proposed rhombic array antenna is designed in Section II. Section III shows the experimental results and discussions. A comparison of the proposed rhombic array antenna and a reference uniformly excited 8 × 10 array antenna is given. At last, the paper is concluded in Section IV.

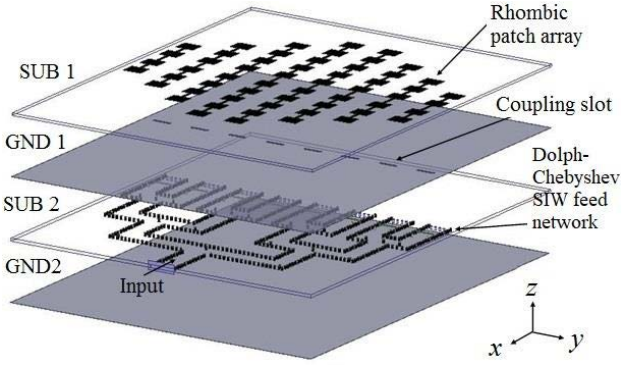

FIGURE 1. 3D view of the proposed 60-GHz rhombic array antenna.

II. DESIGN OF RHOMBIC PATCH ARRAY ANTENNA

Fig. 1 shows the 3D view of the proposed 60-GHz patch array antenna arranged in a rhombic shape (referred to as rhombic array antenna for short). Eight linear serial patch arrays with varying numbers of patches are located on SUB 1. The lower substrate has a −25-dB Dolph-Chebyshev SIW feed network that delivers the input signal to the upper patch through a slot-coupled center-fed structure. SUB 1 uses Rogers 4450F with a thickness of 0.203 mm and a dielectric coefficient of 3.52, while SUB 2 is Rogers 4350B with a thickness of 0.254 mm and a dielectric constant of 3.66. Since the rhombic array changes the number of patches in the E- and H-planes, it can have an equivalent taper excitation, which can reduce its SLL by up to −25 dB, while still maintaining high gain. The following subsections describe the key designs of the proposed array antenna.

A. ARRAY ARCHITECTURE WITH RHOMBIC ARRANGEMENT

An array factor analysis method is proposed to predict the SLL of the antenna. From antenna theory [20], [21], the array factor of an 8 × 10 rectangular array antenna can be expressed as

$$\begin{aligned} AF\ (\theta,\phi)_{\substack{8\times10\\array}} &= \sum_{n=1}^{8}\sum_{m=1}^{10} I_{mn}e^{j\alpha_{mn}}e^{j\psi_{mn}} \\ \alpha_{mn} &= -\beta(x_{mn}\sin\theta_0\cos\phi_0 + y_{mn}\sin\theta_0\sin\phi_0) \\ \psi_{mn} &= \beta(x_{mn}\sin\theta\cos\phi + y_{mn}\sin\theta\sin\phi) \end{aligned} \quad (1)$$

where I_{mn} and ψ_{mn} represent the excitation current and spatial phase delay of the mnth array element, respectively, and θ_0 and ϕ_0 denote the main beam direction. The SLL of an array can be reduced by tapering the current I_{mn}. However, for the series-fed array, changing the I_{mn} requires adjusting the dimensions of all connected segments at the same time, which is very complicated for the design. The proposed rhombic array antenna utilizes quantity ratio to reduce SLL, which can simplify design complexity. The array factor of the rhombic array antenna with in-phase excitation is

$$\begin{aligned} &AF\ (\theta,\phi)_{\substack{rhombic\\array}} \\ &= AF\ (\theta,\phi)_{\substack{8\times10\\array}} - (I_{mn}|_{\substack{m=1,10\\n=3,6}} \\ &\quad + I_{mn}|_{\substack{m=1,2,9,10\\n=2,7}} + I_{mn}|_{\substack{m=1,2,3,8,9,10\\n=1,8}})\, e^{j\psi_{mn}} \end{aligned} \quad (2)$$

Fig. 2(a) shows the architecture of the proposed rhombic array antenna, in which the solid dots represent patches. The rhombic array antenna trims the four corners of the 8 × 10 rectangular array antenna to achieve equivalent taper excitation in both the x and y directions. Fig. 2(b) shows the quantity ratios of the rhombic array in the x-direction (E-plane) and y-direction (H-plane), which are [2:4:6:8:8:8:8:6:4:2] and [4:6:8:10:10:8:6:4], respectively. Fig 3 shows the array factors of the proposed rhombic array antenna and the 8 × 10 rectangular array antenna calculated from (1) and (2) with uniform I_{mn} and equal element spacing of $0.5\lambda_0$, where λ_0 is the free-space wavelength. As shown, the SLL of the proposed rhombic array can be reduced to −22.1 dB, which is much lower than the −12.8 dB of the 8 × 10 rectangular array antenna.

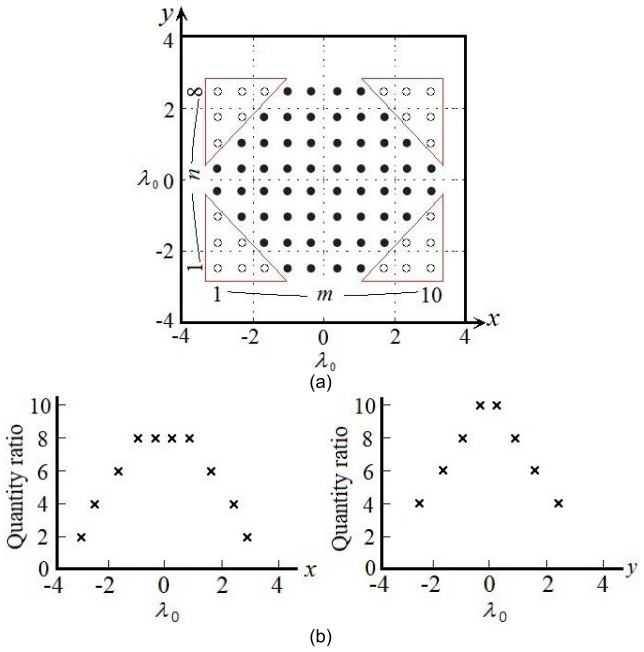

FIGURE 2. (a) Array architecture of the proposed rhombic array antenna. (b) Quantity ratios of the rhombic array in the x- and y-directions.

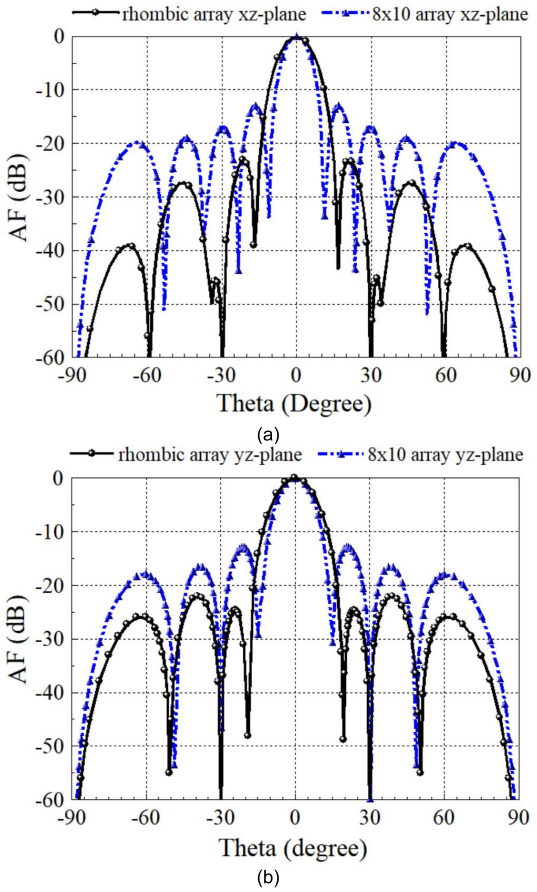

FIGURE 3. Calculated array factors of the proposed rhombic array antenna and 8 × 10 rectangular array antenna: (a) *xz*-plane. (b) *yz*-plane.

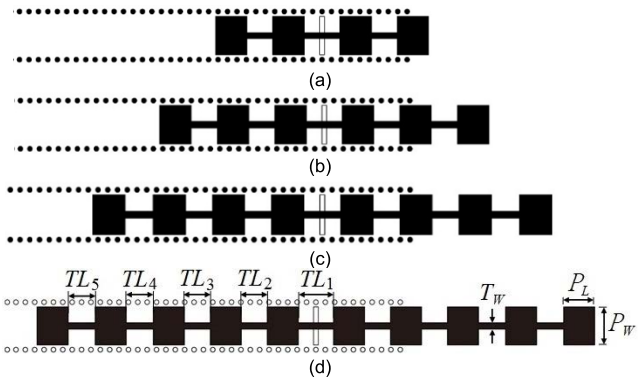

FIGURE 4. Configurations of the linear serial 1 × *N* patch arrays with SIW slot-coupled center-fed structures: (a) 1 × 4, (b) 1 × 6, (c) 1 × 8, and (d) 1 × 10. ($P_L = 1.33$, $P_W = 1.6$, $T_W = 0.27$, $TL_1 = 1.5$, $TL_2 = TL_3 = 1.1$, and $TL_4 = TL_5 = 1.15$, all in mm.)

B. LINEAR SERIAL PATCH ARRAYS WITH SIW SLOT-COUPLED CENTER-FED STRUCTURES

Due to the small size of series-fed structures, this work begins with the linear serial patch array design (referred to as linear array for short). Four 1 × N linear arrays ($N = 4$, 6, 8, 10) are designed to form a rhombic array as shown in Fig. 1. Considering the antenna size and gain requirements, the number of patches of the linear array is limited to ≤10. Fig. 4 shows the configuration of the linear arrays with SIW slot-coupled center-fed structures to simplify the complex feed network required for direct excitation of planar arrays and reduce insertion loss. The dimensions are detailed in the caption of Fig. 4. The length and width of the patch are fixed at 1.33 mm and 1.6 mm, respectively, and the width of the connecting line is fixed at 0.27 mm. The central microstrip line of the linear serial 1 × N patch array is slightly longer due to the influence of the coupling slot below, while the other microstrip connecting lines between patches are almost the same size. When designing an array antenna with different number of elements N, since the circuit size of each part is almost fixed, the required design correction will be quite easy.

When energy is coupled from SIW to a microstrip line, the excitation currents on both sides of the line flow in opposite directions, so the patches will not radiate in phase. To construct the slot-coupled center-fed structure for patch in-phase excitation, it is necessary to design an SIW-to-microstrip anti-phase power splitter. Fig. 5(a) is illustrated with a 1 × 10 linear array where the anti-phase power splitter is marked by a dashed circle. Fig. 5(b) shows the three-port model of this anti-phase power splitter. By adjusting the size and position of the slot, the phase difference between Port 2 and Port 3 can reach 180°. Fig. 6 shows the phase difference of this power splitter. In the frequency range of 57.1∼64.9 GHz, the phase difference of $\angle S_{31} - \angle S_{21}$ is 180°±4.4°, which can meet the design requirements of serial patch arrays. Figs. 7(a)∼7(d) show the simulated radiation patterns at 60 GHz for the proposed 1 × 4 to 1 × 10 linear arrays, with gains of 10.29, 11.71, 12.53, and 13.34 dBi, respectively.

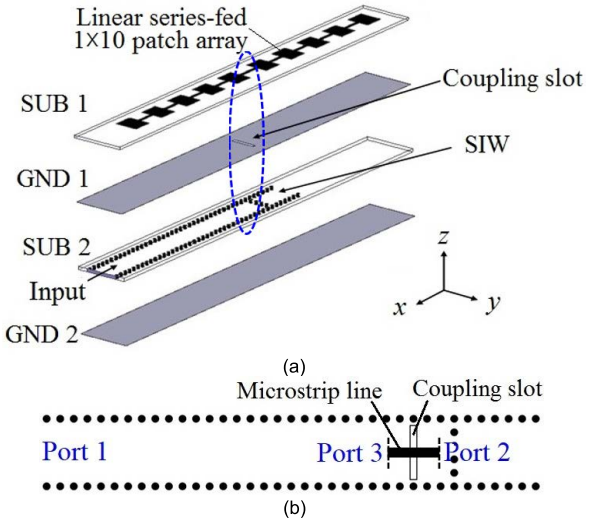

FIGURE 5. (a) 3D view of the linear serial 1 × 10 patch array with a SIW slot-coupled center-fed structure. (b) Three-port model of the SIW-to-microstrip anti-phase power splitter.

From the simulation results, the linear arrays are well designed.

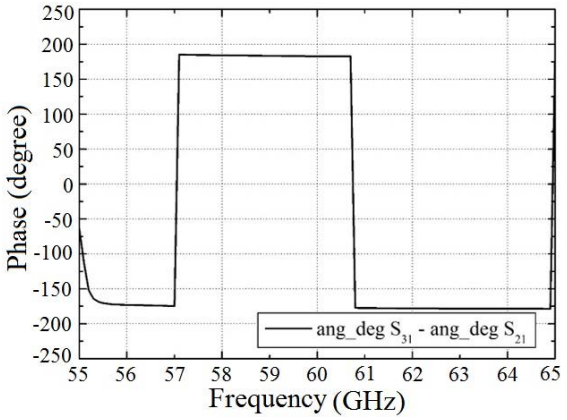

FIGURE 6. Phase difference of the SIW-to-microstrip anti-phase power splitter.

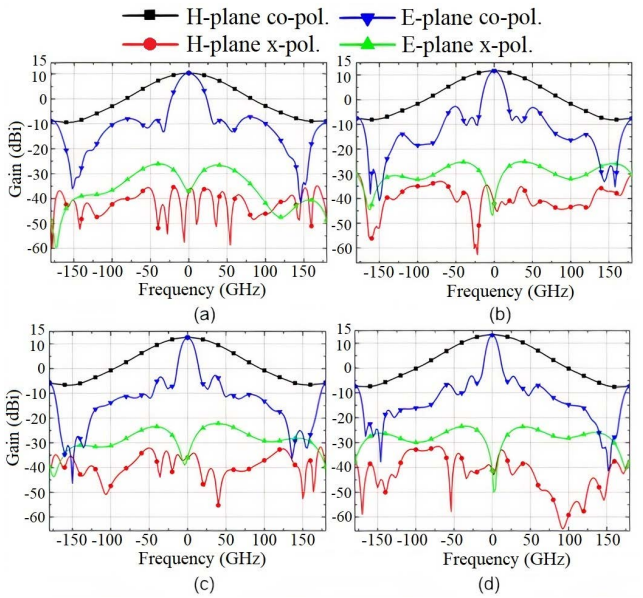

FIGURE 7. Simulated radiation patterns at 60 GHz: (a) 1 × 4 linear array, (b) 1 × 6 linear array, (c) 1 × 8 linear array, and (d) 1 × 10 linear array.

C. 25-dB DOLPH-CHEBYSHEV SIW EIGHT-WAY FEED NETWORK

In order to form a planar array, a −25-dB Dolph-Chebyshev SIW eight-way feed network is designed, which can also be used to further reduce the H-plane SLL of the antenna. A Chebyshev polynomial of order m can be expressed as

$$T_m(z) = \begin{cases} (-1)^m \cosh\left(m\cosh^{-1}(z)\right), & z \le -1 \\ \cos\left(m\cos^{-1}(z)\right), & -1 \le z \le 1 \\ \cosh\left(m\cosh^{-1}(z)\right), & z \ge 1 \end{cases} \quad (3)$$

An array factor consisting of N elements can be approximated by a Dolph-Chebyshev polynomial of order m [20]. Let $m = N - 1$, the array factor can be derived as

$$T_{N-1}(z) = \begin{cases} AF^e = \sum_{n=1}^{M} a_n \cos\left[(2n-1)u\right], & M = N/2, \text{ even} \\ AF^o = \sum_{n=1}^{M+1} a_n \cos\left[(2n-1)u\right], & M = (N-1)/2, \text{ odd} \end{cases} \quad (4)$$

where $u = \pi d\cos\theta/\lambda$ and $AF^{e,o}$ is the array factor. The SLL can be derived as

$$\text{SLL} = T_{N-1}^{Max}(z_0) \quad (5)$$

where $z_0 = z/\cos u$. The Dolph-Chebyshev current ratio can be obtained by setting SLL = −25 dB and $N = 8$. Table 1 lists the current ratios of the eight-element −25-dB Dolph-Chebyshev distribution calculated from (3)∼(5).

Fig. 8 compares the calculated array factor for the −25-dB Dolph-Chebyshev distribution with that of the uniform distribution. The SLL of the Dolph-Chebyshev distribution is less than −25 dB, which is much lower than the −12.8 dB of the uniform distribution. An SIW eight-way feed network with the desired Dolph-Chebyshev distribution can be constructed by using several equal power dividers (EPD) and unequal power dividers (UPD). Table 2 lists the S-parameters required for EPD, UPD1, UPD2, and UPD3 of the feed network.

Fig. 9 shows the configurations of power dividers. To make the feed network symmetrical, EPD is used for the first stage, UPD1 for the second stage, and UPD2 and UPD3 for the third stage. The current ratios required by the output ports of UPD1, UPD2, and UPD3 are calculated as [0.522:1], [0.646:1], and [0.842:1], respectively. The current ratios can be adjusted by the location of the three metallic vias of power dividers as shown in Fig. 9, the dimensions of which are listed in the figure caption.

TABLE 1. Current ratios for the eight-element−25-dB Dolph-Chebyshev distribution.

Element No.	1	2	3	4	5	6	7	8
Theoretical value	0.378	0.584	0.842	1	1	0.842	0.584	0.378
SIW feed network	0.35	0.5	0.8	1	1	0.8	0.5	0.35

Figs. 10 and 11 show the configuration of the SIW eight-way feed network and its simulated S-parameter responses, respectively. The S-parameters of the eight output ports of the feed network are quite consistent in phase, and their amplitude difference can meet the design requirements of power splitting. Table 1 also lists the current ratios inversely derived from the simulated S-parameters of the SIW feed network, which are very close to the theoretical values of Dolph-Chebyshev distribution. Fig. 8 also compares the array

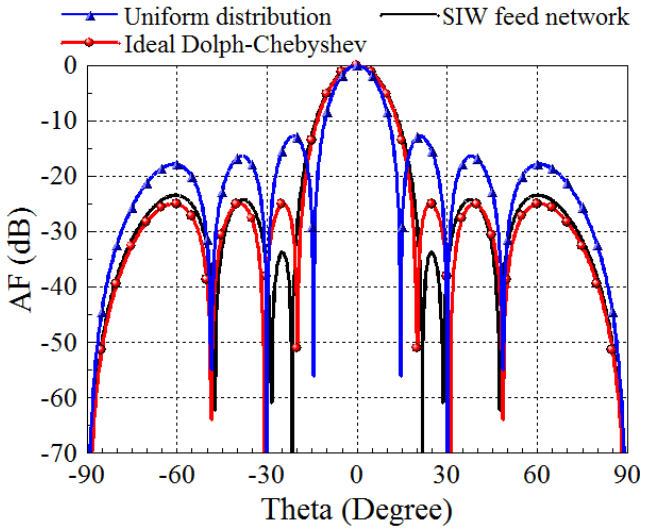

FIGURE 8. Calculated array factors of the eight-element −25 dB Dolph-Chebyshev distribution with an element spacing of $0.5\lambda_0$.

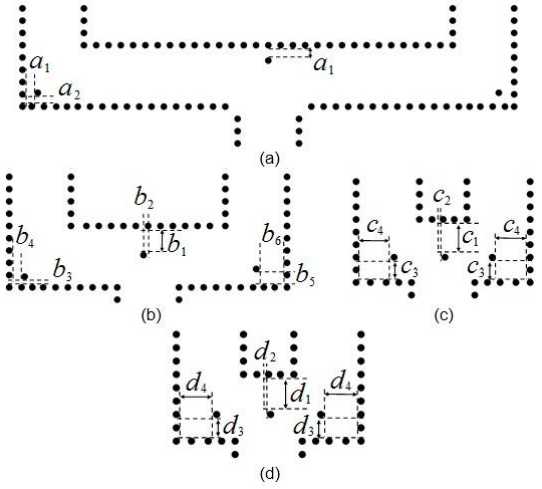

FIGURE 9. Configurations and size parameters of the power dividers: (a) EPD. (b) UPD1. (c) UPD2. (d) UPD3. ($a_1 = 0.3$, $a_2 = 0.25$, $b_1 = 0.75$, $b_2 = b_3 = 0.15$, $b_4 = 0.3$, $b_5 = 0.4$, $b_6 = 0.8$, $c_1 = c_4 = 1$, $c_2 = 0.06$, $c_3 = 0.6$, $d_1 = d_4 = 1$, $d_2 = 0.04$, and $d_3 = 0.6$, all in mm).

TABLE 2. *S*-Parameters required for EPD and UPDs of the SIW eight-way feed network.

Power divider	EPD	UPD1	UPD2	UPD3
S-parameters of output ports (dB)	−3/ −3	−1.04/ −6.69	−1.51/ −5.31	−2.32/ −3.81
Amplitude difference (dB)	0	5.65	3.8	1.49

factor of the constructed SIW feed network, which is close to the theoretical result with a maximum SLL of less than −23.5 dB.

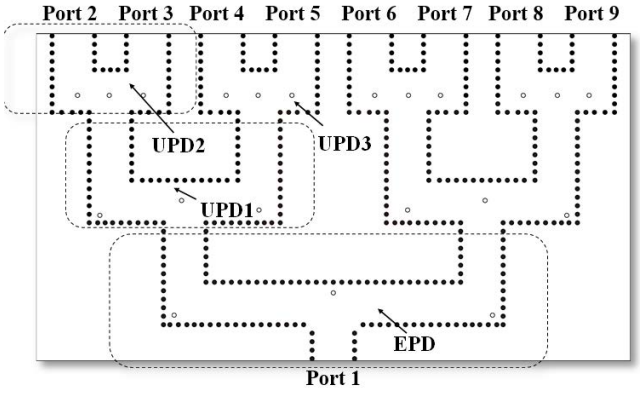

FIGURE 10. Configuration of the −25-dB Dolph-Chebyshev SIW eight-way feed network.

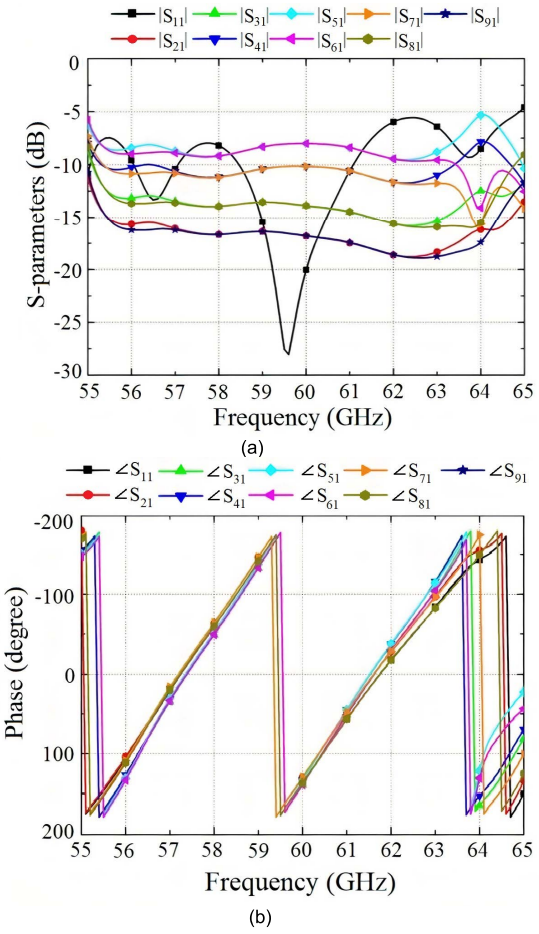

FIGURE 11. *S*-parameters of the −25-dB Dolph-Chebyshev SIW eight-way feed network: (a) Magnitude. (b) Phase.

Fig. 12 shows the top view of the proposed 60-GHz antenna, where eight linear arrays are symmetrically arranged along the H-plane with a quantity ratio of [4:6:8:10:10:8:6:4] to form a rhombic planar array. The center of each linear array is aligned with the coupling slot of the SIW feed network. Parametric analysis is required because the slot will affect the coupling energy and impedance matching. In our

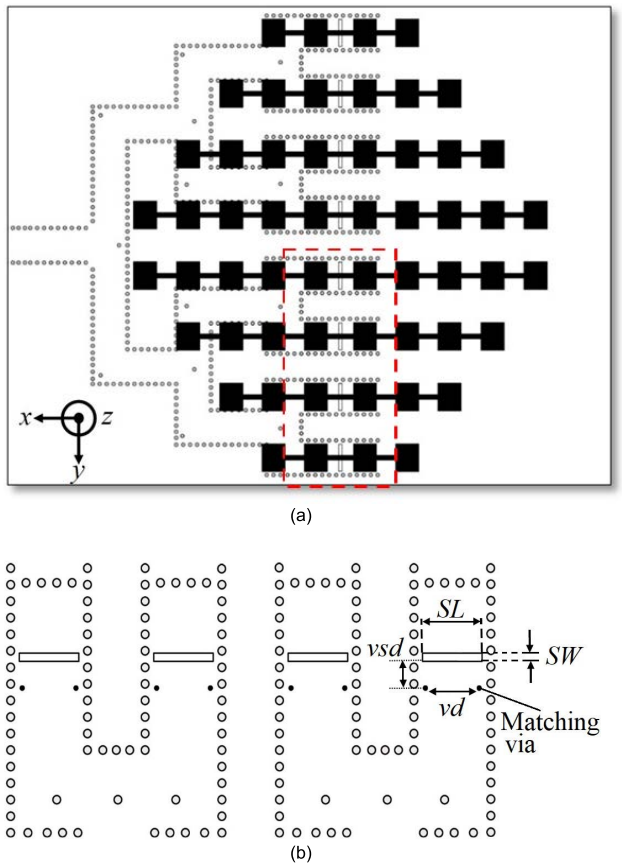

FIGURE 12. Proposed 60-GHz rhombic array antenna: (a) Top view, (b) Enlarged view of the marked circuit in Fig. 12(a) with patches removed. (*SL* = 1.55, *SW* = 0.1, *vd* = 1.4, and *vsd* = 0.345, all in mm.)

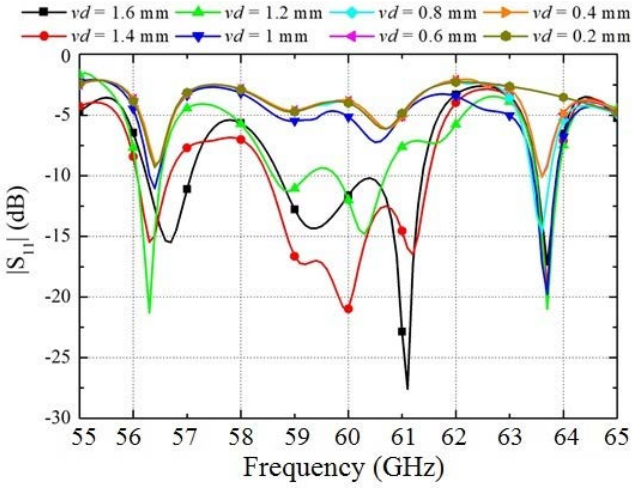

FIGURE 13. Simulated S_{11} responses corresponding to the change of the matching via pitch *vd*.

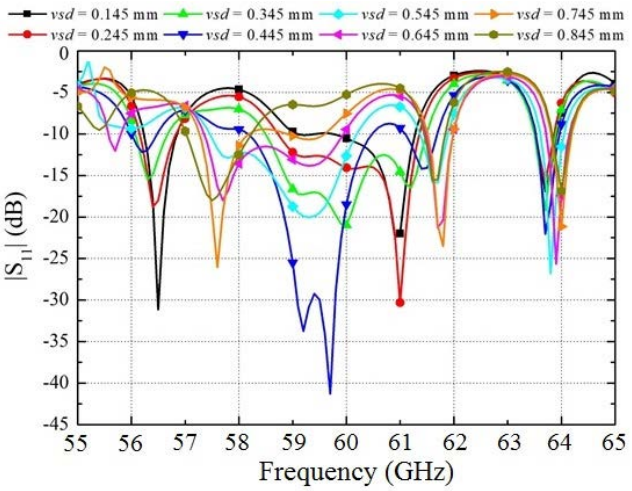

FIGURE 14. Simulated S_{11} responses corresponding to the change of the matching via position *vsd*.

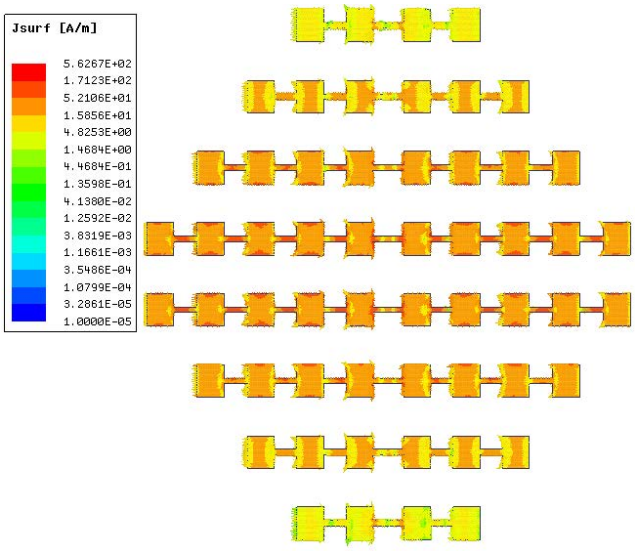

FIGURE 15. Surface current distribution of the proposed rhombic array antenna.

study, slot length *SL* slightly longer than half wavelength and narrower slot width *SW* will have better performance. However, the effect of only adjusting *SL* and *SW* is very limited. The bandwidth can only reach 0.4% and the return loss is small. Therefore, two matching vias are added to improve the bandwidth.

Figs. 13 and 14 show the simulated S_{11} responses for varying the pitch *vd* and the position *vsd* of the matching vias, respectively. As shown, the bandwidth can be increased significantly when *vd* is 1.4 mm and *vsd* is 0.345 mm. The final selected size is detailed in the caption of Fig. 12. According to the simulation results of S_{11}, the bandwidth can be increased to 58.49∼61.49 GHz (or 5%).

Fig. 15 shows the surface current distribution of the proposed antenna. In the H-plane, the current tapers off to both sides as expected due to the −25-dB Dolph-Chebyshev SIW feed network, while in the E-plane, the current variation is small since each linear array is uniformly excited.

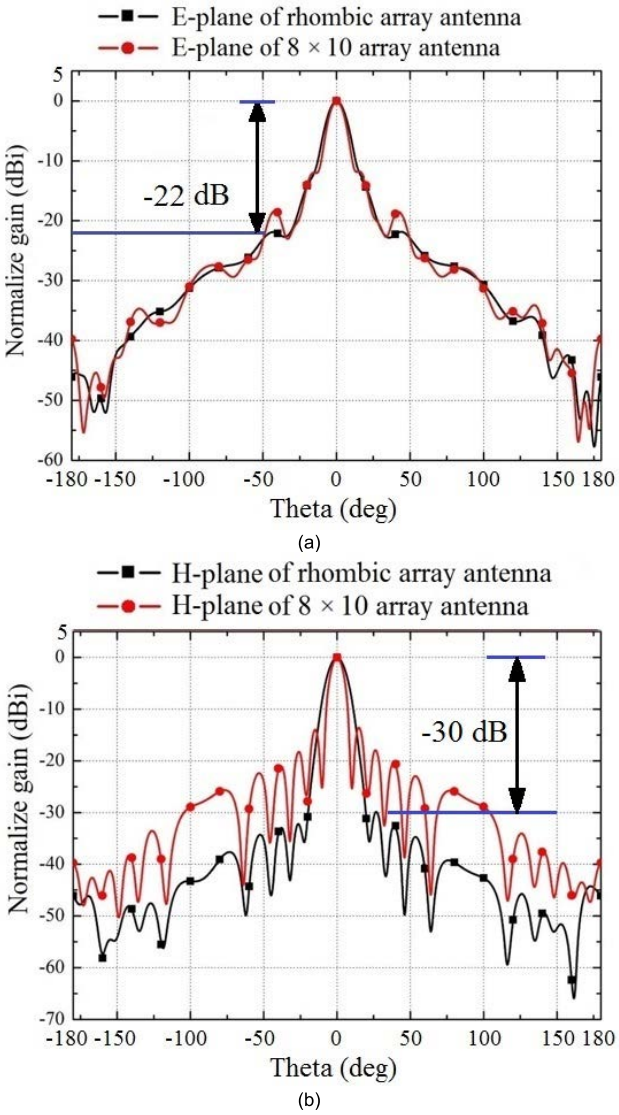

FIGURE 16. Simulated normalized radiation patterns of the proposed rhombic array antenna and the reference high-gain 8 × 10 rectangular array antenna: (a) E-plane. (b) H-plane.

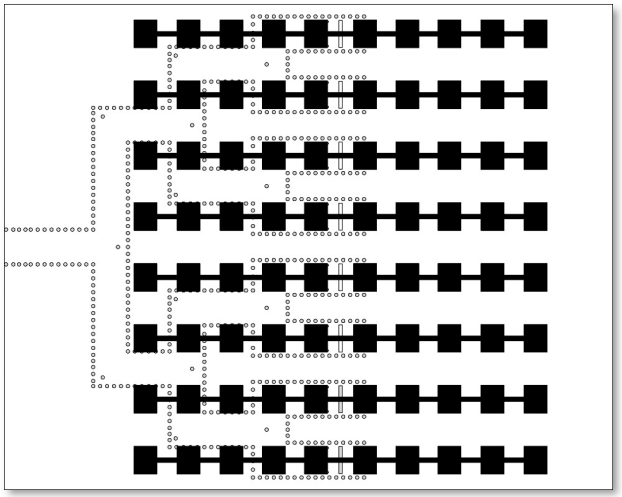

FIGURE 17. Reference uniformly excited high-gain 8 × 10 rectangular array antenna.

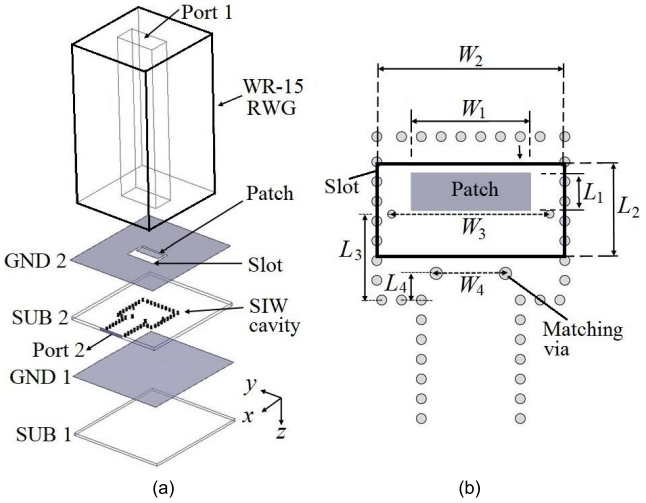

FIGURE 18. Configuration of the input port with RWG-to-SIW transition: (a) 3D view and (b) Enlarged view ($W_1 = 2.4$, $W_2 = 2.8$, $W_3 = 3.2$, $W_4 = 1.4$, $L_1 = 0.75$, $L_2 = 1.85$, $L_3 = 1.74$, and $L_4 = 0.54$, all in mm.)

III. EXPERIMENTAL RESULTS AND DISCUSSIONS

A. COMPARISON OF THE PROPOSED RHOMBIC ARRAY ANTENNA AND A REFERENCE HIGH-GAIN 8 × 10 ARRAY ANTENNA

Fig. 16 shows the simulated normalized radiation patterns of the proposed rhombic array antenna at 60 GHz with a gain of 19.8 dBi. In the H-plane, the SLL can be reduced to −30 dB due to both the quantity ratio of patches and the Dolph-Chebyshev feed network. Since the E-plane pattern is only improved by the quantity ratio of patches, its maximum SLL is reduced to −22 dB, occurring at ±44°.

For comparison, a reference high-gain 8 × 10 rectangular array antenna is also designed in this work as shown in Fig. 17, which is uniformly excited by an SIW eight-way equal power divider. Fig. 16 also includes the radiation patterns of this reference array antenna with a simulated gain of 20.8 dBi which is 1 dB higher than the proposed rhombic array antenna. Since the reference array antenna does not introduce any design to reduce the SLL, the E-plane and H-plane SLLs are only −12 dB and −13.6 dB, respectively.

As shown in Fig. 16, the curve of the proposed rhombic array antenna is smoother than that of the reference array antenna. Since the proposed rhombic array antenna requires only 56 patches, the array area can be reduced by 23%.

B. INPUT PORT WITH RWG-TO-SIW TRANSITION

Since the input interface of the measurement system is a WR-15 rectangular waveguide (RWG), the input port of the proposed antenna requires a transition structure from RWG to SIW [22]. Fig. 18 shows the configuration of the input port with RWG-to-SIW transition with dimensions listed in the

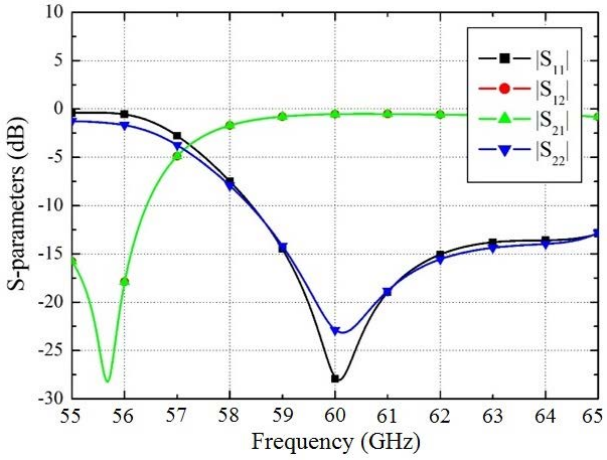

FIGURE 19. Simulated *S*-parameter responses of the input port with RWG-to-SIW transition.

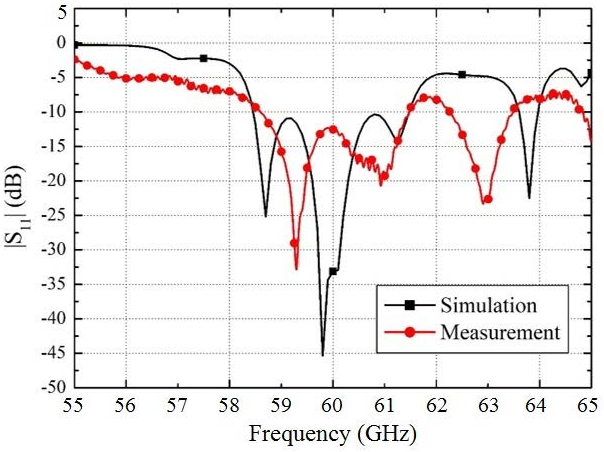

FIGURE 21. Simulated and measured *S*-parameters of the proposed rhombic array antenna with RWG-to-SIW transition and a WR-15 adapter.

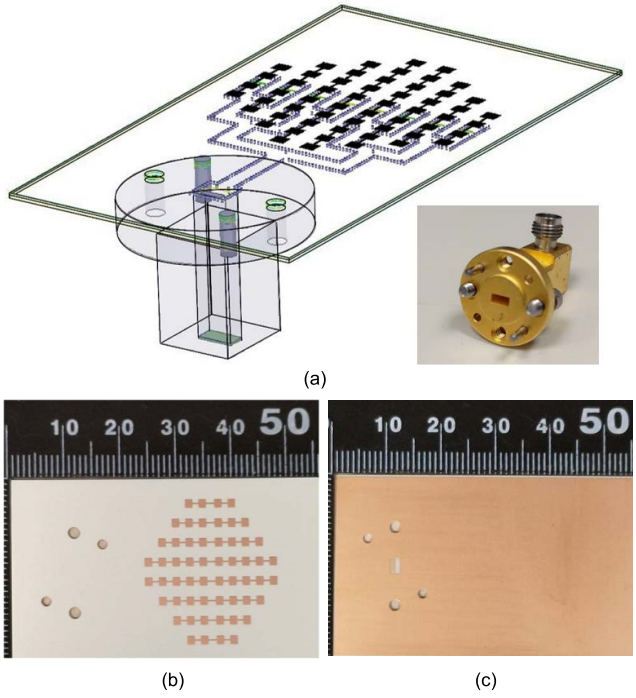

FIGURE 20. Proposed rhombic array antenna with RWG-to-SIW transition and a WR-15 RWG-to-coax adapter: (a) 3D view. (b) Top-view photograph. (c) Bottom-view photograph.

caption. Due to the different distribution of electromagnetic fields in RWG and SIW, it is necessary to add an additional SIW cavity, arrange a metalic patch inside the slot, and place four matching vias near the slot, so that the electromagnetic field can be transferred smoothly.

Fig. 19 shows the simulated *S*-parameters of the input port with RWG-to-SIW transition, where Port 1 and Port 2 are the RWG and SIW terminals, respectively. From the simulated results, the 10-dB impedance bandwidth is from 58.4 to 65 GHz, the insertion loss is only −0.54 dB, and the S_{11} and S_{22} are both lower than −22 dB at 60 GHz, showing quite good performance.

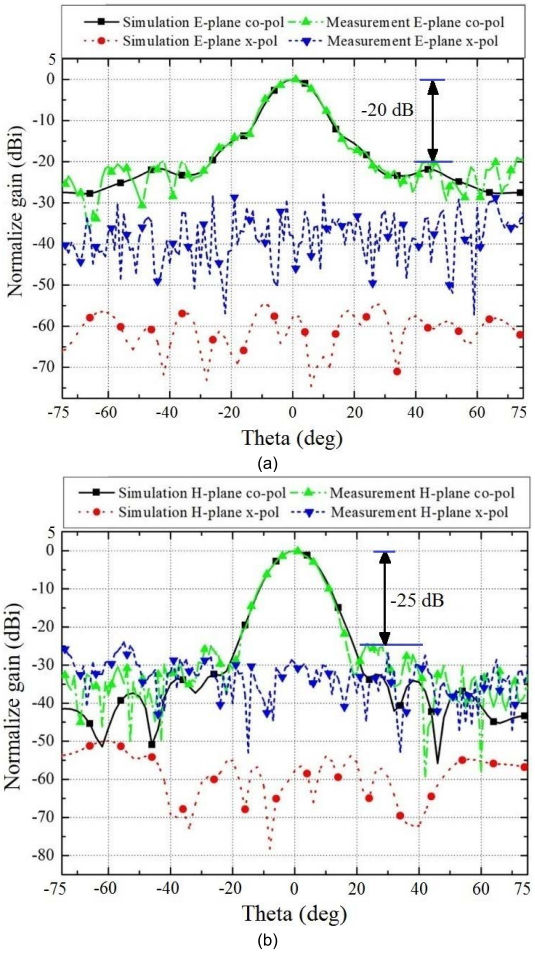

FIGURE 22. Simulated and measured radiation patterns of the rhombic array antenna with RWG-to-SIW transition and a WR-15 adapter: (a) E-plane. (b) H-plane.

C. EXPERIMENTAL RESULTS

For verification, a complete rhombic array antenna was fabricated and measured in this work. Fig. 20 shows the photographs of the proposed antenna with RWG-to-SIW

TABLE 3. Performance comparison of the proposed antenna and the previously reported low-sll antennas.

Ref.	f_0 (GHz)	Pol.	Element type	Distribution	No. of element	Peak gain (dBi)	$\|S_{11}\|$ BW (%)	SLL E/H-plane (dB)	Cross-pol. (dB)
[1]	28.25	Linear	Patch	Taylor	1×8	13.97	8.1	−18.3[a](E-plane)	−20[a]
[2]	10	Linear	Slot	Taylor	10×10	22	4	−32.3/−33.8	NP
[3]	25.3	Linear	Patch	PSO	16	12.03	1.4	−7.57(E-plane)	NP
[4]	14	CP	A-shaped element	Taylor	1×10	12.3 dBic	2.9 (AR-BW)	−19.1	NP
[5]	4	CP	Patch	Sequential rotation	4×4	NP	20	−17.5[a](D-plane)	−20
[7]	28	Dual	Slot	Taylor	16×16	28	5(y-pol.) 5.2(x-pol.)	−18.5(y-pol.) −19.5(x-pol.)	−30
[10]	3.44	Linear	Slot	Dolph-Chebyshev	5×4	18.2	0.6[a]	−20/−20	−42
[12]	76.5	Linear	Patch	Dolph-Chebyshev	1×8	13.8	3.9[a]	−17(E-plane)	NP
[14]	14.25	Linear	Patch	DEA	1×8	16.1	12.56	−20.3(H-plane)	NP
[15]	5.8	CP	Patch	WCMMPTE	12	15.3 (dBic)	12.4(AR-BW)	−30	−30[a]
[17]	6.2	Linear	Patch	EAD	9	14.8	7.4	−23.8/−24.1	NP
This work	**60**	**Linear**	**Patch**	**Rhombic array + Dolph-Chebyshev**	**56**	**18.2**	**4.7**	**−20/−25**	**−30**

Abbreviation: CP = circularly polarized, BW = bandwidth, SLL = sidelobe level, Cross-pol. = cross-polarization, NP = not provided, AR-BW = axial ratio-bandwidth, DEA = differential evolution algorithm, EAD = equivalent amplitude distribution, PSO = particle swarm optimization, WCMMPTE = weighted constrained method of the maximum power transmission efficiency. [a]Calculated from the graph of the referenced paper.

transition and a WR-15 RWG-to-coax adapter. The S_{11} of the proposed antenna was measured using an Anritsu MS4647B vector network analyzer with a 1.85 mm coaxial calibration kit (Anritsu 3654D), while the radiation patterns were measured by an in-house far-field millimeter-wave antenna measurement system [23] calibrated using a standard gain horn (Millitech SGH-15-RP000).

Fig. 21 shows the simulated and measured results for S_{11}. The simulated and measured 10-dB impedance bandwidths are 58.46 to 61.47 GHz (or 5%) and 58.6 to 61.5 GHz (or 4.7%), respectively, which are in good agreement. Fig. 22 shows the simulated and measured normalized radiation patterns. Due to the limitation of the mechanical bracket of the measuring equipment, the measuring angle is limited within ±75°. From the simulated results, the gain is 19.8 dBi, and the SLLs of the E-plane and H-plane are −21.6 dB and −32 dB, respectively. The measured gain is 18.2 dBi, and the measured SLLs of the E-plane and H-plane are −20 dB and −25 dB, respectively. The cross-polarization level is less than −30 dB. The discrepancy between the measured and simulated SLLs is small in the E-plane but noticeable in the H-plane. Inferred from further simulated results, the discrepancy in the H-plane may be caused by manufacturing errors in the SIW feed network, resulting in out-of-phase and incorrect amplitude ratios of the excitation currents for each linear array. However, the −25 dB SLL is still acceptable for most applications. Fig. 23 shows the measured and simulated realized gain curves. Both curves have similar fluctuations, but the measured gain curve is slightly shifted towards low frequencies. Overall, the gain curve is fairly smooth with little variation.

The comparison of the proposed rhombic array antenna with the previously reported low-SLL antennas is shown in Table 3. It can be seen that the proposed antenna has the advantages of high peak gain and low SLL at high operating

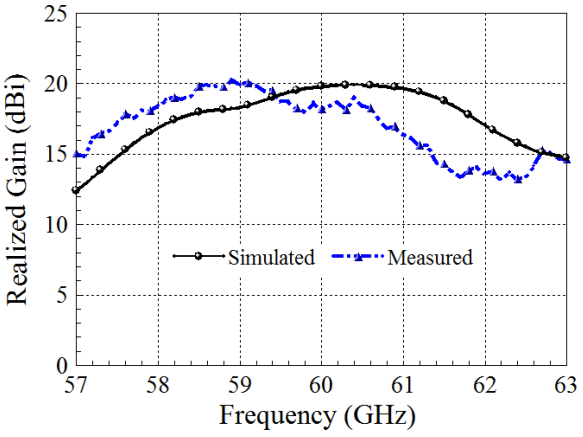

FIGURE 23. Simulated and measured realized gains of the proposed rhombic array antenna.

frequency of 60 GHz. In addition, the proposed antenna utilizes the quantity ratio of patches for equivalent taper excitation to reduce SLL, rather than the use of tapered width as in traditional designs, which can achieve high gain and avoid cumbersome resizing of patches and connecting lines.

IV. CONCLUSION

This work presents a 60-GHz rhombic patch array antenna with high gain, low SLL, and reduced array area. This antenna is designed based on eight linear serial arrays with varying number of patches. A SIW slot-coupled center-fed structure is designed to avoid the complex feed network required for direct excitation of planar arrays and reduce insertion loss. The equivalent taper excitation in the E-plane and H-plane directions is achieved by the quantity ratio of patches, which can obtain high gain and avoid cumbersome resizing of patches and connecting lines. Array factor analysis

is carried out to predict the SLL of the antenna. A −25-dB Dolph-Chebyshev distribution SIW eight-way feed network is design to form the planar array and further reduce the H-plane SLL. The measured results show that the proposed antenna has a gain of 18.2 dBi, and the SLLs in the E-plane and H-plane are less than −20 dB and −25 dB, respectively. This work also simulates a reference uniformly excited high-gain 8 × 10 array antenna, compared to which the proposed rhombic array antenna has similar simulated gain but much lower SLL and 23% smaller array area.

REFERENCES

[1] S.-J. Park, D.-H. Shin, and S.-O. Park, "Low side-lobe substrate-integrated-waveguide antenna array using broadband unequal feeding network for millimeter-wave handset device," *IEEE Trans. Antennas Propag.*, vol. 64, no. 3, pp. 923–932, Mar. 2016.
[2] H. Yang, G. Montisci, Z. Jin, Y. Liu, X. He, and G. Mazzarella, "Improved design of low sidelobe substrate integrated waveguide longitudinal slot array," *IEEE Antennas Wireless Propag. Lett.*, vol. 14, pp. 237–240, 2015.
[3] A. R. Gutiérrez, A. Reyna, L. I. Balderas, M. A. Panduro, and A. L. Mendéz, "Nonuniform antenna array with nonsymmetric feeding network for 5G applications," *IEEE Antennas Wireless Propag. Lett.*, vol. 21, no. 2, pp. 346–350, Feb. 2022.
[4] Y. Zhang, Y. J. Cheng, Y. F. Wu, and Y. Fan, "Low-sidelobe-level circularly polarized short leaky-wave antenna with A-shaped element based on substrate integrated image guide," *IEEE Antennas Wireless Propag. Lett.*, vol. 21, no. 2, pp. 272–276, Feb. 2022.
[5] A. B. Smolders and H. J. Visser, "Low side-lobe circularly-polarized phased arrays using a random sequential rotation technique," *IEEE Trans. Antenna Propag.*, vol. 62, no. 12, pp. 6476–6481, Dec. 2014.
[6] G. Zhou, Q. Liang, and B. Sun, "Design of short backfire antenna arrays with high gain and low sidelobe level," in *Proc. 6th Asia–Pacific Conf. Antennas Propag. (APCAP)*, Oct. 2017, pp. 1–3.
[7] J. Ran, C. Jin, P. Zhang, W. Wang, and Y. Wu, "High-gain and low-loss dual-polarized antenna array with reduced sidelobe level based on gap waveguide at 28 GHz," *IEEE Antennas Wireless Propag. Lett.*, vol. 21, no. 5, pp. 1022–1026, May 2022.
[8] Y. Q. Wen, B. Z. Wang, and X. Ding, "A wide-angle scanning and low sidelobe level microstrip phased array based on genetic algorithm optimization," *IEEE Trans. Antennas Propag.*, vol. 64, no. 2, pp. 805–810, Feb. 2016.
[9] D. Zarifi, A. Farahbakhsh, and A. U. Zaman, "A V-band low sidelobe cavity-backed slot array antenna based on gap waveguide," in *Proc. 14th Eur. Conf. Antennas Propag. (EuCAP)*, Mar. 2020, pp. 1–3.
[10] R.-S. Chen, L. Zhu, S. W. Wong, X. Z. Yu, Y. Li, L. Zhang, and Y. He, "Low-sidelobe cavity-backed slot antenna array with simplified feeding structure for vehicular communications," *IEEE Trans. Veh. Technol.*, vol. 70, no. 4, pp. 3652–3660, Apr. 2021.
[11] M. Aruga, M. Zhang, J. Hirokawa, and M. Ando, "Low-sidelobe design of a waveguide reflection-canceling slot array antenna in the 60 GHz band," in *Proc. Int. Symp. Antennas Propag. (ISAP)*, 2016, pp. 360–361.
[12] Y. Kang, E. Noh, and K. Kim, "Design of traveling-wave series-fed microstrip array with a low sidelobe level," *IEEE Antennas Wireless Propag. Lett.*, vol. 19, no. 8, pp. 1395–1399, Aug. 2020.
[13] B. Li, Y. Qiu, J. Zhang, Y. Deng, Z. Zhou, and L. Sun, "W-band high-gain hybrid-fed microstrip patch array with low sidelobe patterns," in *Proc. Int. Conf. Microw. Millim. Wave Technol. (ICMMT)*, Sep. 2020, pp. 1–3.
[14] F. Zhang, T. Xu, and M. Yao, "Low sidelobe coupled broadband microstrip array antenna with non-uniform spacing and variable groove length," *IEEE Access*, vol. 8, pp. 184451–184456, 2020.
[15] Y. Dong, X. Cai, and G. Wen, "Circularly polarized antenna array with suppressed sidelobes for electronic toll collection," *IEEE Antennas Wireless Propag. Lett.*, vol. 21, no. 5, pp. 988–992, May 2022.
[16] M. W. Niaz, Z. Ahmed, and M. B. Ihsan, "Performance comparison of different aperture shapes for microstrip reflectarray," in *German Microw. Conf. Dig. Papers*, 2010, pp. 250–253.
[17] H. Yang, T. Li, L. Xu, X. Cao, J. Gao, J. Tian, H. Yang, and D. Sun, "A new strategy to design microstrip antenna array with low side-lobe level and high gain," *IEEE Access*, vol. 7, pp. 152715–152721, 2019.
[18] J. G. Joshi, S. S. Pattnaik, S. Devi, M. R. Lohokare, and C. Vidyasagar, "Offset fed diamond shaped split ring (DSSR) planar metamaterial antenna," in *Proc. Appl. Electromagn. Conf. (AEMC)*, Dec. 2009, pp. 1–4.
[19] W. A. W. Muhamad, R. Ngah, M. F. Jamlos, P. J. Soh, and H. Lago, "Gain enhancement of microstrip grid array antenna for 5G applications," in *Proc. URSI Asia–Pacific Radio Sci. Conf. (URSI AP-RASC)*, 2016, pp. 1827–1829.
[20] R. L. Haupt, Antenna Arrays: A Computational Approach, Hoboken, NJ, USA: Wiley, 2010.
[21] C. A. Balanis, *Antenna Theory Analysis and Design*, 2nd ed. Hoboken, NJ, USA: Wiley, 1997.
[22] I. Mohamed and A. Sebak, "Broadband transition of substrate-integrated waveguide-to-air-filled rectangular waveguide," *IEEE Microw. Wireless Compon. Lett.*, vol. 28, no. 11, pp. 966–968, Nov. 2018.
[23] K.-S. Chin, W. Jiang, W. Che, C.-C. Chang, and H. Jin, "Wideband LTCC 60-GHz antenna array with a dual-resonant slot and patch structure," *IEEE Trans. Antennas Propag.*, vol. 62, no. 1, pp. 174–182, Jan. 2014.

CHI-EN TSAI was born in Taipei, Taiwan. He received the B.S. and M.S. degrees in electrical engineering from Chang Gung University, Taoyuan, Taiwan, in 2019 and 2021, respectively. His research interests include microwave circuits and antennas.

HUAYAN JIN (Member, IEEE) was born in Hangzhou, Zhejiang, China, in 1989. She received the B.S. and Ph.D. degrees from the Nanjing University of Science and Technology (NUST), Nanjing, China, in 2011 and 2017, respectively. From August 2012 to January 2013, from May 2013 to October 2013, and from April 2014 to October 2014, she was an Exchange Student with Chang Gung University, Taoyuan, Taiwan.

Since May 2017, she has been with Hangzhou Dianzi University, where she is currently an Associate Professor. Her main research interests include microwave and millimeter-wave antennas, differential-fed antennas, and filtering antennas.

CHAO-HSIANG LIAO received the Ph.D. degree in communication engineering from the National Taiwan University, Taipei, Taiwan, in 2010.

From August 2012 to July 2019, he has served as the Technical Leader for SGS Global OTA, New Taipei, Taiwan. He was focusing on CTIA/3GPP RAN4 contributions for SISO/MIMO/5G NR mmWave OTA. Since December 2013, he has been serving as a Secretary for the CTIA MIMO OTA Sub-Working Group. From February 2014 to September 2021, he has also served as a Secretary for the CTIA OTA Measurement Uncertainty Sub-Working Group. He was responsible for CTIA test plan discussion, draft, edition, and monthly meeting summary. From August 2019 to July 2020, he was with the faculty of the Department of Electrical Engineering, Lunghwa University of Science and Technology, Taoyuan, Taiwan, where he has served as an Assistant Professor. Since August 2020, he has been the Technical Leader of SGS Global OTA, SGS. Since April 2021, he has been serving as a Manager for the SGS Taiwan Neihu Antenna Laboratory, responsible for the administrative management and OTA/SAR technical support. Since October 2021, he has been serving as the Co-Chair for the CTIA OTA Measurement Uncertainty Sub-Working Group. His research interests include antenna design and OTA measurement (SISO/MIMO/5G NR mmWave).

CHUNG-YI LI (Senior Member, IEEE) received the B.S., M.S., and Ph.D. degrees in electrical engineering from the National Tsing Hua University, Taiwan, in 1996, 1998, and 2011, respectively. He is currently an Associate Professor with the Department of Electronics Engineering and the Center for Reliability Sciences Technologies, Chang Gung University, and the Department of Radiation Oncology, Chang Gung Memorial Hospital-Linkou, Taiwan. His research interests include IC design and testing, random number generator, power electronics, fault-tolerant design, FPGA-based implementation of digital control, phase locked loop design, antenna design, and power IC.

WEI-CHIH CHANG was born in Hsinchu, Taiwan. He is currently pursuing the B.S. degree in electronic engineering with Chang Gung University. His research interests include microwave circuits and antennas.

HUAI-EN LIU was born in Taipei, Taiwan. He is currently pursuing the B.S. degree in electronic engineering with Chang Gung University. His research interests include microwave circuits and antennas.

KUO-SHENG CHIN (Senior Member, IEEE) received the B.S. degree in electrical engineering from the Chung Cheng Institute of Technology, Taoyuan, Taiwan, in 1986, the M.S.E.E. degree from Syracuse University, Syracuse, NY, USA, in 1993, and the Ph.D. degree in communication engineering from the National Chiao Tung University, Hsinchu, Taiwan, in 2005.

From 1986 to 2005, he was with the Chung Shan Institute of Science and Technology, Taoyuan, as a Research Assistant, becoming an Assistant Scientist and then an Associate Scientist. He joined Chang Gung University, Taoyuan, as a Faculty Member, in 2006, where he is currently a Professor with the Department of Electronic Engineering. He has supervised a student team to win first place in the 2009 National Electromagnetism Application Innovation Competition, Taiwan. His current research interests include microwave and millimeter-wave couplers, filters, duplexers, low-temperature cofired ceramic circuits, automotive radar antennas, frequency-selective surfaces, filtering antennas, radomes, and electromagnetic pulse research. He was one of the recipients of the Best Paper Award of the International Conference on Electromagnetic Near Field Characterization and Imaging, in 2009, the Honorable Paper Award of the International High Speed Intelligent Communication Forum, in 2010, the Best Student Paper Award of the International Symposium on Next-Generation Electronics, in 2014, the Best Paper Award of the Taiwan Precision Engineering Workshop, in 2016, and the Best Student Paper Award of 2018 The 8th International Symposium on InfoComm and Mechatronics Technology in Bio-Medical and Healthcare Application. He received the Outstanding Teacher Award from Chang Gung University, in 2014 and 2021. He served as an Associate Editor for *Microwave and Optical Technology Letters*, from 2019 to 2020.